Carrier-selective p- and n-contacts for efficient and stable photocatalytic water reduction

Bae, Dowon; Pedersen, Thomas; Seger, Brian; Iandolo, Beniamino; Hansen, Ole; Vesborg, Peter Christian Kjærgaard; Chorkendorff, Ib

Published in:
Catalysis Today

Link to article, DOI:
10.1016/j.cattod.2016.11.028

Publication date:
2017

Document Version
Peer reviewed version

*Graphical Abstract (for review)

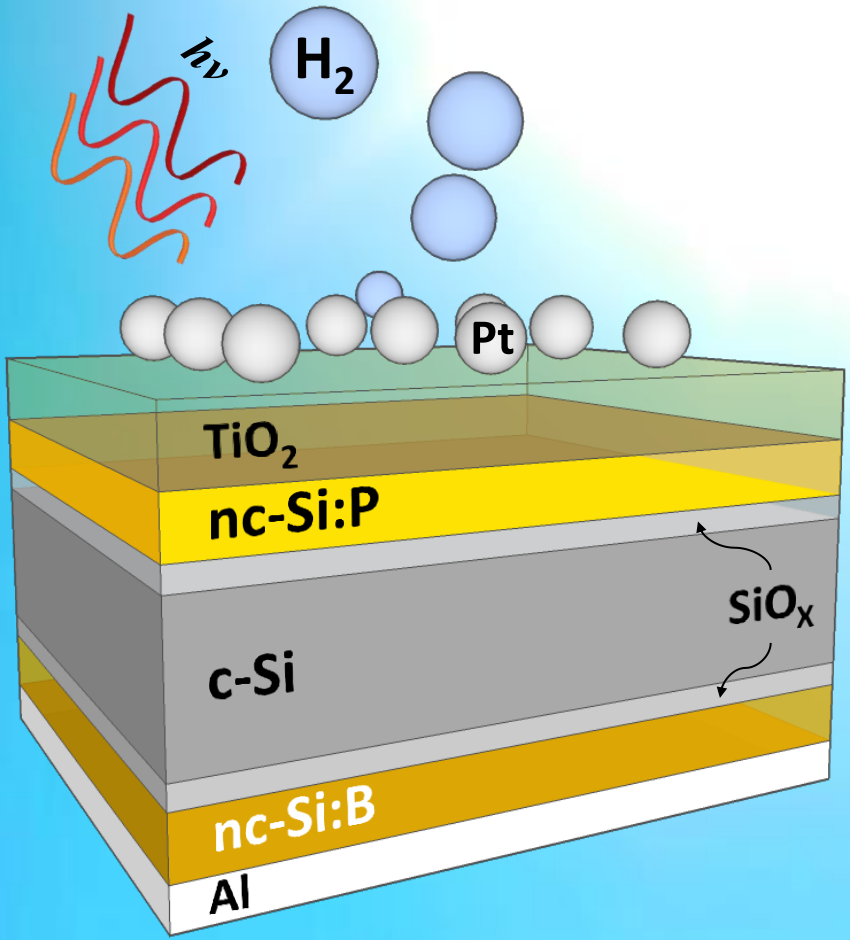

Carrier-selective p- and n-contacts for efficient and stable photocatalytic water reduction

Dowon Bae[1], Thomas Pedersen[2], Brian Seger[1], Beniamino Iandolo[3], Ole Hansen[1,2], Peter C.K. Vesborg[1], Ib Chorkendorff[1†]

[1]VILLUM Center for Science of Sustainable Fuels and Chemicals, Department of Physics, Technical University of Denmark, Building 311, Fysikvej, DK-2800 Kgs, Lyngby, Denmark

[2]Department of Micro- and Nanotechnology, Technical University of Denmark, DK-2800 Kgs. Lyngby, Denmark.

[3]Center for Electron Nanoscopy, Technical University of Denmark, DK-2800 Kgs. Lyngby, Denmark.

[†]*Corresponding author E-mail: ibchork@fysik.dtu.dk; Tel: +45) 45 25 31 70; Fax: +45) 45 93 23 99*

Keywords: photocatalysis, carrier-selective contact, hydrogen evolution, metal-oxide-semiconductor

Abstract

The successful realization of carrier-selective contacts for crystalline silicon (c-Si) based device for photocatalytic hydrogen production has been demonstrated. The proposed TiO_2 protected carrier-selective contacts resemble a metal-oxide-semiconductor configuration, including a highly-doped nanocrystalline silicon (nc-Si) and a tunnel oxide, thereby form a heterostructure with the c-Si substrate. By substituting conventional pn^+-junction Si by c-Si/SiO_X/nc-Si structure for both front and back contacts we demonstrate a 16% increase in photovoltage (an open circuit voltage of 584 mV under AM 1.5G conditions). TiO_2 protected carrier-selective photoelectrodes showed excellent long-term durability in acidic aqueous solution having stable photocurrent output for more than 40 days, implying that the proposed carrier-selective contact is a promising configuration to substitute for the conventional pn-junction based c-Si photocathodes.

1. Introduction

Photoelectrochemical splitting of water into H_2 (and O_2) could become a key technology for making clean, sustainable fuels [1,2]. However, solar water splitting with a photoelectrochemical (PEC) cell has severe problems to overcome before commercialization is realistic. The most important problem is perhaps the efficiency. 2-photon device (tandem-) structures that use two different band gap materials (one with a wide gap combined with a

narrow gap) are optimally suited to maximize efficiency since the photovoltage provided by these optimized devices almost perfectly matches the voltage needed to split water [3–5]. In the case of the narrow E_g material, recent theoretical work has shown that Si has suitable E_g and band alignments for the photocathode of a tandem water splitting device [6,7]. Also, efficient H_2 production (HER) with open circuit voltage above 0.5 V and photocurrent in excess of 20 mA cm^{-2} has been shown experimentally using pn^+-Si photocathode with a homojunction architecture with a Pt co-catalyst [8–10]. However, the current state-of-the-art Si PEC photoelectrodes are still far from the theoretical limits [11] which suggests a different approach is needed than the traditional Si pn-homojunction. To date, substantial effort been made to improve the performance of Si-based photocathodes [7–10,12–16]. Above all, carrier-selective contact designs borrowed from metal-oxide-semiconductor (MOS) Si solar cells have recently come into the spotlight because of their efficient carrier transport and low recombination rate [12,13,15]. One of the outstanding examples of this approach is the use of polycrystalline silicon (pc-Si) having ITO/pc-Si/SiO_2/p-Si heterojunction photovoltaic (PV) cell by Feldmann *et al.* which reached an open circuit voltage (V_{OC}) above 690 mV and a short-circuit current density (J_{SC}) of 30 mA cm^{-2}, due to minimized minority carrier recombination [17,18]. The key features of this structure are chemical surface passivation of the silicon by SiO_2, in the form of a thin tunnelling interlayer, and selective carrier transport due to an energy barrier for majority carrier created by highly doped pc-Si. This PV–approach, however, cannot be used directly for PEC application, since photoelectrodes are operated in corrosive electrolytes, and thus need to be protected from corrosion [3,8]. Si-based photoanodes coupled to protective metal oxides, such as Ir/TiO_2/n-Si [19] and NiO_X/Ni/SiO_2/n-Si [20], are examples which have shown rather good stability in the electrolytes (8 and 12 h, respectively) with an open circuit photovoltage (V_{ph}) above 500 mV under oxygen evolution reaction (OER) conditions. Scheuermann *et al.* recently demonstrated a PV-assisted hybrid type MOS Si photoanode coupled with Ir (Ir/TiO_2/SiO_2/p^+n-Si) for OER

which showed V_{ph} above 600 mV in in ferri-/ferrocyanide [21]. In spite of above-mentioned successes in OER, very little work has been done studying photocatalytic HER with a MOS structure. Talin's group demonstrated HER using Pt/Ti/SiO_2/p-Si with V_{oc} of 490 mV [15], and L. Ji *et al.* demonstrated a Pt/Ti/$SrTiO_3$/p-Si structure for the improved long-term stability (~ 35 hours in 0.5M H_2SO_4) yielding on V_{oc} of 450 mV [13]. However, these designs have limited photocurrent density due to light absorption by the metallic layers, and their HER performance has yet to show results that are superior to conventional (homojunction)-based Si photocathodes. Moreover, minimal energy level analysis has been done to understand how the carriers can be selectively injected from the MOS to the solid/liquid interface.

In this work we apply a c-Si/SiO_X/nc-Si structure approach to both front- and back contacts, which provide interface passivation and selective injection of minority- and majority carrier to the conducting protective layer and back contact, respectively. The main focus is on evaluation of the impact on photocathodic performance of passivating, carrier-selective back- and front contacts compared to conventional pn^+-(homo) junction based Si photocathode. A transparent TiO_2 film was sputtered on top of the highly doped nc-Si as a conducting protection layer, and Pt nanoparticles were subsequently drop-cast on the samples for photocatalytic hydrogen evolution in 1M $HClO_4$.

Using thin-film Si as a metallic layer has been employed in recent state-of-art MOS based PV cells [18,22], however this approach has not been utilized in the more demanding photoelectrode application. Moreover, the detailed working principles based on the band energy analysis are outlined to understand how the carriers can be injected selectively and transferred to solid/liquid interface in PEC system.

2. Methods

2.1. Sample fabrication

Si based photocathodes were fabricated using 350 μm thick CZ c-Si wafers (Topsil, 1-20 ohm-cm, boron-doped, acceptor density $N_A \approx 5 \cdot 10^{15}$ cm^{-3}) as a substrate, on which thin SiO_X

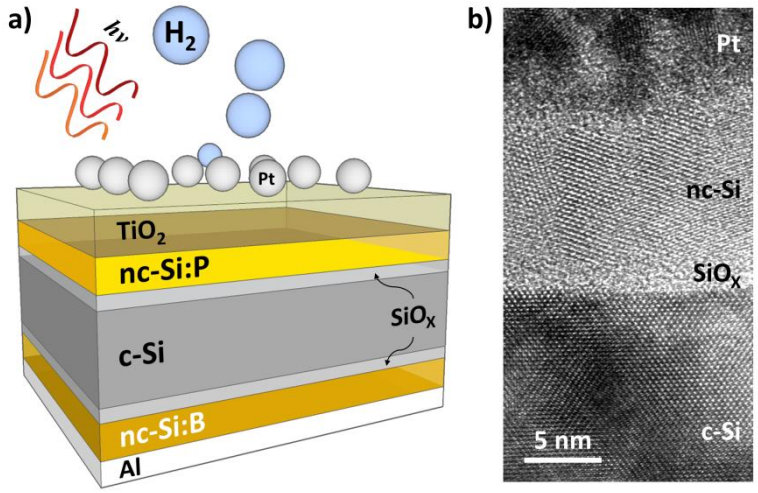

Figure 1. Schematic cross section of the device architecture with carrier-selective contacts used for photocatalytic activity (HER) experiments in this work (a). The light is illuminating the TiO_2 side. (b) HRTEM bright field image of a cross-section of the front side of a similar device without a TiO_2 layer, which shows the carrier-selective contact (c-Si/SiO_X/nc-Si).

(~ 1.5 nm) layers were chemically grown on RCA (Radio Corporation of America) cleaned [23] c-Si by oxidation in 68% HNO_3 solution at 95˚C for 10 min. Next, the nc-Si films were grown at 580˚C in a low-pressure chemical vapour deposition (LPCVD) furnace at 200 mTorr with a 80 sccm silane flow and a 7 sccm PH_3 or B_2H_6 flow, depending on the conductivity type (n^+ or p^+), resulting in growth of either 15 nm or 50 nm of n^+ or p^+ nc-Si layers (nc-Si:P and nc-Si:B,) respectively. Subsequently, the samples were annealed at 800˚C for an hour in an atmospheric pressure tube furnace under N_2 flow. The n^+ nc-Si:P is on the illuminated (front) side of the sample and the thickness is kept low (15 nm) to minimize parasitic photon loss in this layer. The p^+ nc-Si:B layer is on the non-illuminated (back) side and the thickness does not matter for optical losses. Therefore, the back side thickness is increased to 50 nm to be able to accommodate reactions with Al during annealing, *i.e.* to make sure that annealing does not result in a usual Al/Si back contact. A mesa-isolated [8] nc-Si/SiO_2/c-Si structure (hereafter denoted as a carrier-selective contact) with a plateau height of 3 μm was formed at the front side by photolithography and dry etching (Here, we used SF_6, O_2 and C_4F_8 gases in a "Pegasus" Deep Reactive Ion Etching system from SPTS Technologies). A metallic charge collecting layer was deposited on the backside at room temperature by e-beam evaporation of

Al, then a Cu-wire was attached to it using Ag-paste as an electrical connect as described elsewhere [10]. In order to prevent corrosion or passivation of the Si surface a TiO_2/Ti (100/5 nm) protection layer was sputtered onto the n^+ nc-Si using previously published methods [8,10]. The metallic Ti interlayer was deposited to prevent the Si surface from oxidation during the TiO_2 deposition process as described elsewhere [8,10,24]. The schematic drawing of cross-sectional structure of the sample is shown in Figure 1a, and a high resolution transmission electron microscope (HRTEM) image presented in Figure 1b shows that an amorphous SiO_x phase is present between the bulk c-Si and the thin nc-Si layer. Some samples received a 30-minute annealing at 420˚C in forming gas (5% H_2 + 95% Ar; FG from now on) before or after the TiO_2 deposition to improve the passivation quality of the oxide layer [25,26]. The surface was cleaned using a "piranha" solution (3:1 mixture of H_2SO_4 (98%) and H_2O_2 (35%) solutions), then rinsed with Millipore water and dried. Pt was used as a co-catalyst for HER by having 2.5 μg per cm^2 of a dinitrosulphatoplatinate solution drop-casted on the TiO_2 surface as described elsewhere [8,10]. In some samples, conventional homogeneous pn^+-junction Si was formed in the same manner as in previous works [10] for use as control samples. All samples were sealed with epoxy (Loctite 1C Hysol) yielding an exposed surface area of approximately 0.2 cm^2 (individually measured using the optical image analysis program ImageJ 1.46r).

2.2. Characterization

A 1000 W Xenon lamp (Oriel) was used either with an AM1.5 filter or an AM1.5 filter in addition to a 635 nm cut-off filter (*i.e.* $\lambda > 635$ nm to simulate the wavelengths and intensity which would be received by the narrow E_g cell of the tandem device [10]). The light intensity reaching the sample was measured via a spectroradiometer (Ocean Optics Inc, USB4000), and a Bio-Logic VSP potentiostat was used using EC Lab software for photoelectrochemical measurements. All cyclic voltammetry (CV) experiments were done in a 3 electrode H-cell in

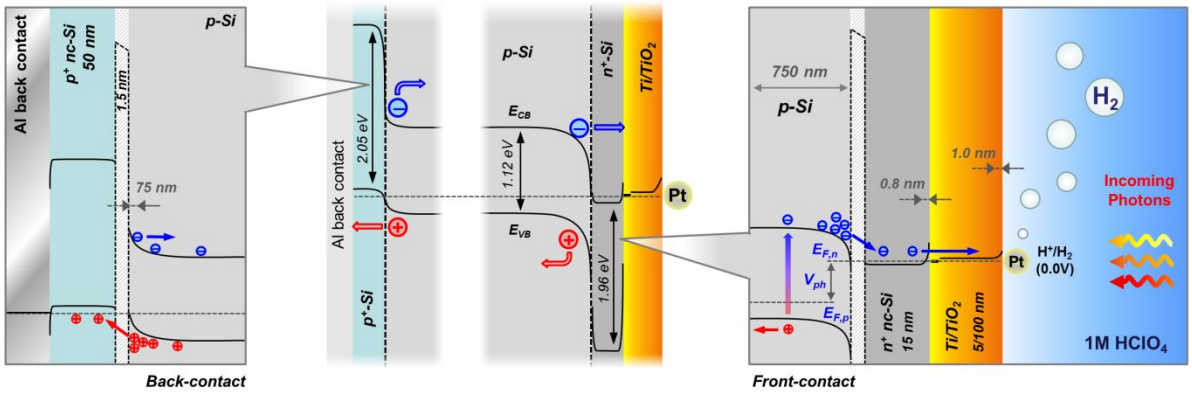

Figure 2. Schematic band diagram of the sample in equilibrium with H^+/H_2 reaction. The diagram calculation procedure and required values for calculation can be found in the supporting information (Figure S1) of this work and elsewhere [8,10,27]. Note that values with grey and black arrow correspond to the depletion width and band gap, respectively.

an aqueous 1M $HClO_4$ (Aldrich 99.99%) electrolyte. For all CV's the electrodes were scanned at a sweep rate of 10 mV sec^{-1}.

A Pt mesh was used as a counter electrode and the reference was a saturated $Hg/HgSO_4$ electrode (Schott Instruments). The solution was purged with H_2 gas for approximately 20 minutes prior to any experiment. In order to determine the stability of the photocatalytic HER activity, the photocathode was evaluated by conducting chronoamperometry (CA) experiments under the same operating conditions used to perform the CV experiments for 41 days. The working potential for the long term CA was chosen as the position of the maximum power point of the electrode.

To determine band gap of nc-Si and TiO_2 thin films, optical transmission measurements were performed using an integrating sphere (Mikropack ISP-50-8-R-GT). The formation of nc-Si/SiO_X/c-Si structure was verified with *ex situ* HRTEM (Titan 80-300, FEI) imaging at an accelerating voltage of 300 kV.

3. Results and discussion

As shown in Figure 1b, HR-TEM image of the nc-Si/SiO_X/c-Si interface shows that amorphous SiO_X phase is formed between the bulk and thin film Si layer. Figure 2 depicts the schematic energy diagram of the carrier-selective sample in equilibrium with H^+/H_2 reaction.

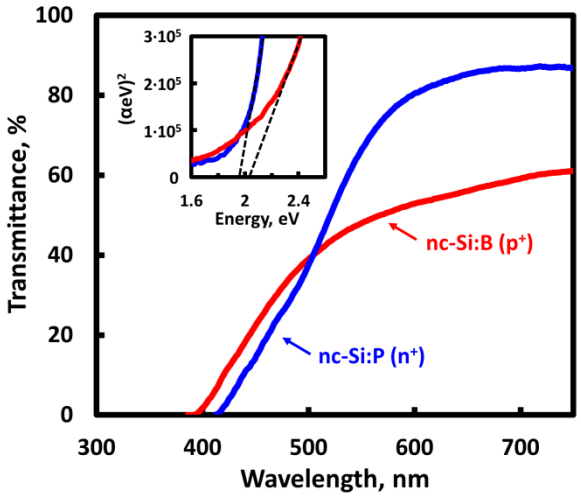

Figure 3. Transmittance spectra of n^+-and p^+-doped nc-Si deposited on a quartz substrates as optical characterization samples. The signal from the quartz substrate was subtracted as a background spectrum. Tauc plot converted from the transmittance to estimate its band gap also shown as an inset.

This description relies on basic solid state physics principles and simplifies the understanding of how electron–hole pairs can be separated by a built-in electric field and then selectively transferred to the appropriate interface. The depletion layer thicknesses can be calculated as a function of voltage (see SI). This allows for the depletion layers through the device to be drawn in Figure 2. The detailed energy diagram and its calculation procedure can be found in supplementary content (SI)[‡]. The photo-generated electrons are swept away from the bulk silicon by a potential drop (downward band bending) at the negatively-charged inversion layer, which also repels holes. The electrons can then tunnel through the SiO_X into the conduction band of the TiO_2 and ultimately to the platinum electrocatalyst. At the back-contact, the opposite is true and an upward band bending sweeps the holes away and reflects the electrons back into the bulk [18]. The band bending distance in the highly doped n^+ nc-Si (phosphorus doped nc-Si) region was found to be approximately 0.8 nm. The high dopant density from the nc-Si should easily allow for electronic tunnelling from the Si to the Ti metallic layer [27]. From the previous Mott-Schottky analysis [8,10,24], the TiO_2 conduction band (CB) was determined to be -0.05 V vs. RHE with a donor density level of 10^{20} cm^{-3}, and the depletion width of the TiO_2 at the interface was determined to be around 1.0(2) nm. As shown in Figure

3, LPCVD deposited nc-Si films have a direct band gap of approximately 2.0 eV, which is likely due to hydrogenation of the silicon layers during the chemical gas reaction. The difference in apparent band gap for the two CVD grown films is probably due to different sizes of the nano-crystallites in the two materials. Generally, the crystallites of boron doped Si (p^+ nc-Si) are smaller than phosphorus doped one (n^+ nc-Si), resulting in an increased band gap [28,29].

The effects of carrier selective contacts on the PEC properties of the photocathodes were evaluated by measuring CV in 1M $HClO_4$ under illumination (Figure 4), and the measured values are shown in Table 1. A photocathode with a carrier selective back contact and a conventional pn^+-(homo)junction as a front junction (CS-1) showed considerable enhancement in V_{ph} (approximately 27 mV) with a comparable FF (63.6%) to that of the conventional pn^+-Si control sample. The improvement can be explained by the fact that the thin tunnel oxide (SiO_2) layer at the back contact simultaneously reduces interface recombination of majority carriers [18] and provides a barrier to reflect minority carriers back into the bulk as illustrated in Figure 2. Another configuration using carrier selective contacts both at the back and front interfaces (CS-2) gives a V_{ph} of approximately 20 mV with respect to the sample CS-1, reaching a value of ~536 mV vs. RHE, showing that the conventional homogeneous pn^+-junction was successfully substituted by the heterogeneous MOS junction. Similarly to the previous back contact case (*i.e.* CS-1), we attribute this further increase in V_{ph} and J_L to improved surface passivation and enhanced minority carrier injection. The CV data indicates that both the p^+ nc-Si and the n^+ nc-Si layer provide a reasonably low resistance pathway, since the overall series resistance of the device is comparable to that of a conventional pn^+-Si control device. These results demonstrate that adding highly doped nc-Si carrier selective contacts provide good passivation of both contacts. Besides improving photovoltage, the good optical transparency of the phosphorous doped n+ nc-Si thin film

architecture also improves the saturation photocurrent as fewer photons are absorbed before reaching the pure, bulk silicon.

Table 1. Structure of samples used in present work and PEC performance under light illumination.

Structure	Light[1]	*FG*	V_{OC}, mV	J_L[2], mA cm^{-2}	*FF*, %
Control sample (Control)					
Al/pn$^+$-Si/Ti/TiO_2/Pt	Red	No	489	21.2	60.4
Carrier selective back contact (CS-1)					
Al/nc-Si:B/SiO_X/pn$^+$-Si/Ti/TiO_2/Pt	Red	No	516	22.1	63.6
Carrier selective back & front contacts (CS-2)					
	Red	No	536	22.7	55.3
Al/nc-Si:B/SiO_X/p-Si/SiO_X/nc-Si:P/Ti/TiO_2/Pt	Red	Yes	571	23.6	62.7
	White	Yes	584	33.2	61.3

[1] *White and red light correspond to the simulated light with AM1.5G and AM 1.5G with 635 nm cut-off filters, respectively.*
[2] *Note that J_L corresponds to the photocurrent value measured at 0V vs. RHE.*

An interesting phenomenon is that the fill factor (FF) of the CS-2 sample significantly decreased to 55.3% even though the V_{ph} and J_L of the CS-2 configuration surpass those of the CS-1 and the control. Particularly, the CV curve of CS-2 shows an increased slope in the saturation photocurrent region, whereas the slope near open-circuit voltage point is quite similar to the other samples. This strongly indicates the presence of shunt paths. Since the photocathode sample CS-2 with a carrier selective contact only at the back side showed a relatively flat slope in saturation current region, it seems that the decrease of the shunt resistance is mainly attributed to processing techniques on the top layers. One potential cause could be imperfect SiO_2 growth on the Si surface, which could lead to direct contact of c-Si with P-doped nc-Si layer. However, this effect is probably negligible, since the CS-1 sample also had this same procedure done on one of its interfaces, and the results show no noticeable shunt resistance. Alternatively, this shunt resistance could be related to defects formed during the TiO_2 sputtering process. I.e. Sputtering damage could be sustained be the the P-doped nc-Si and/or SiO_2 layers forming shunt paths. As a mitigation method, a forming gas (FG) annealing process was chosen. This is a well-known defect passivation treatment for Si devices since it saturates trap sites in the damaged film with hydrogen atoms [22,30]. As

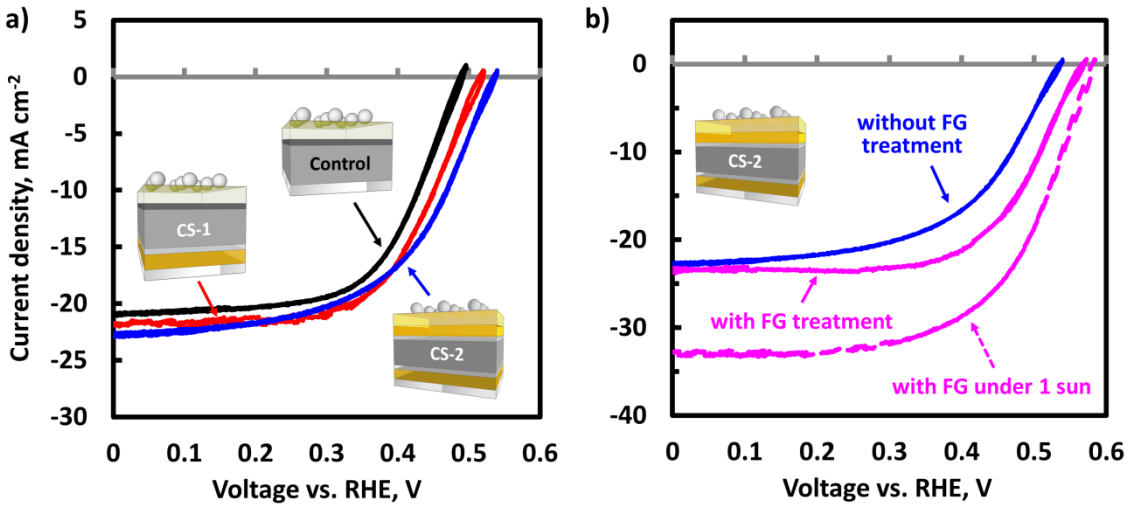

Figure 4. CVs of Si photocathodes (a) with conventional pn^+-junction (control; black), carrier-selective contact at the back side (CS-1; red), and carrier-selective contacts at both front and back side (CS-2; blue) under red light ($\lambda \geq 635$ nm; 38.6 mW cm^{-2}). CS-2 sample showed improved photocatalytic HER performance after FG treatment (b) having V_{ph} of 572 mV with increased fill factor (64%). Note that CV curve with dashed purple corresponds to the CS-2 sample under full spectrum with AM 1.5G filter (100 mW cm^{-2}).

shown in Figure 4b, sample CS-2 with FG post-annealing treatment exhibits an additional V_{ph} of 37 mV, reaching a value of ~571 mV vs. RHE with comparable FF (62.7%) to that of control sample and CS-1, whereas CS-2 with FG annealing treatment prior to the TiO_2 protection layer deposition process shows no significant change in CV curves (Figure S2). The FG treatment for Si-based device is widely used [9,19,21], and the FG annealing effect and on performance of the MOS-based device are discussed in previous studies [22,26,31]. Nevertheless, our results suggest that the sputtering process for deposition of the TiO_2 protection layer is a critical step which may damage the carrier-selective contact.

It is also worth noticing that under AM1.5 full spectrum the CS-2 electrode showed a V_{ph} of 584 mV with J_L of ~33.2 mA cm^{-2}. To the best of our knowledge, this is among the highest V_{ph} and J_L observed for a lab scale c-Si based photocathode performing HER (note that M. Kast *et al.* showed a V_{ph} of 618 mV using commercial c-Si cell [14]). In particular, rapid increase in photocurrent resulted in a maximum power point (V_{Pmax}) of 0.43 V representing a FF above 61%, which is amongst the highest values attained on MOS-based c-Si photocathodes for HER. A high fill factor is extremely important for high efficiency

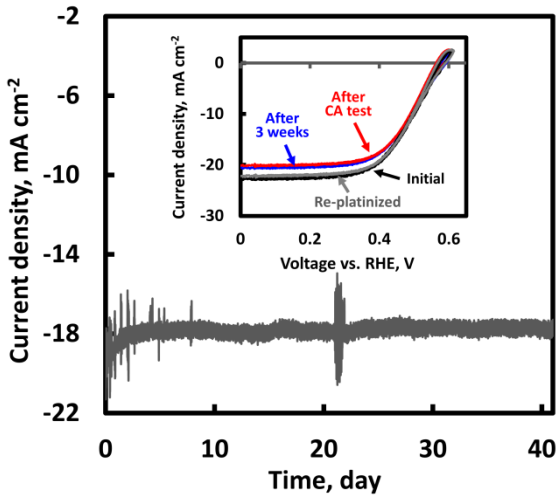

Figure 5. CA of the FG treated CS-2 sample measured at 0.4 V vs. RHE in 1M $HClO_4$. Initial CV prior to the CA measurement (black), CV after 3 weeks (blue), after 41 days (red), and CV from a re-platinized sample after the long-term CA test (grey) also can be found in inset.

photoelectrcatalytic water splitting devices because it has a dramatic effect on the solar-to-hydrogen efficiency due to the steep increase in operating photocurrent densities [32]. Interestingly, the observed photocurrent is lower than expected considering the irradiance of the full spectrum (~ 42 mA cm^{-2} under 100 mW cm^{-2} [10]), and this is likely partially due to the finite light absorption property of the nc-Si layer (Figure 3a) and the water absorption [33] at the low wavelength range.

Figure 5 shows the long-term photocatalytic HER stability at a fixed applied potential (0.4 V versus RHE) of the forming gas treated CS-2 photoelectrode. It can be seen that the sample showed initial degradation during the first day likely due to loss of Pt [24] and/or adsorption of impurities [8]. However, no clear sign of further degradation was observed for the following 40 days of continuous illumination confirming a stabilized photocurrent of 18 mA cm^{-2} (with red light illumination). To discern if the degradation in current was caused by the catalyst loss and/or absorption of impurities, a CV test for the re-platinized sample was done under the same operating conditions. Since the CV of the re-platinized sample recovered its photocatalytic activity, the initial degradation in photocurrent is not attributed to the degradation of the Si device. Note that the sample surface was rinsed with deionized water and piranha solution prior to the re-platinization to remove any organic impurities that may

have accumulated as previously described [8,24]. It is interesting that the onset potential stayed the same, while the saturation current increased after the cleaning and re-platinization. In comparing this long-term stability result to our previous work on ALD (atomic layer deposition) TiO_2 protected pn^+-Si [24], an interesting difference is evident. In the present work the sample showed stable photocurrent for more than 40 days, whereas in the ALD case the sample showed gradual decrease in photocurrent starting after 20 days. We attribute this to different encapsulation: In the present work, the sample was encapsulated with epoxy, whereas back-side of the sample in the previous work [24] was encapsulated with Ethylene-vinyl acetate (EVA) based hot-melt glue, which may decompose during a long-term stability test in a highly oxidizing acid environment.

4. Conclusions

We have demonstrated that the c-Si/SiO_X/nc-Si is an efficient carrier selective contact design and that coupling with a TiO_2 protection layer is suitable for photocathodic hydrogen production in an acidic aqueous solution. By comparing with the control pn^+-Si photocathode, improved photovoltage and photocurrent were achieved because of the built-in energy barrier formed by oxide and wide gap nc-Si layers, leading to the selective injection of minority and majority carrier to solid/liquid interface and back contact, respectively. Interestingly, a forming gas annealing treatment resulted in additional improvement in performance reaching V_{ph} of 584 mV (571 mV with 635 nm cut-off filter), which is the highest value reported to date for a MOS-based c-Si photocathode under HER condition. Furthermore, long-term photostability of the sample with carrier selective contacts over 40 days showed that this device architecture is promising to successfully substitute the conventional pn-junction based Si photoelectrode. However, plenty of room remains for optimizing process parameters, since the-state-of-the-art PV cell with similar design shows V_{ph} of 690 mV indicating that despite the good performance achieved, there is still a further ~100 mV to be had from a Si-based photocathode.

Acknowledgements

The authors acknowledge the support of the Danish Council for Independent Research (DFF-4005-00463), and the support by the VILLUM Center for Science of Sustainable Fuels and Chemicals which is funded by VILLUM Fonden (20805). B. Iandolo acknowledges financial support from the People Programme (Marie Curie Actions) of the European Union's Seventh Framework Programme (FP7/2007-2013) under REA Grant Agreement No. 609405 (COFUNDPostdocDTU). The authors also thank Zoltan Balogh for the assistance with preparing of the lamella for TEM inspection.

‡Supplementary information available: Supplementary figures and dataset can be found in supporting information - Band bending calculation procedure; CV curve for the control sample after FG treatment.

[1] H. Döscher, J.L. Young, J.F. Geisz, J.A. Turner, T.G. Deutsch, Solar-to-hydrogen efficiency: shining light on photoelectrochemical device performance, Energy Environ. Sci. 9 (2016) 74–80. doi:10.1039/C5EE03206G.

[2] S. Dahl, I. Chorkendorff, Solar-fuel generation: Towards practical implementation, Nat. Mater. 11 (2012) 100–101. doi:10.1038/nmat3233.

[3] B. Seger, I.E. Castelli, P.C.K. Vesborg, K.W. Jacobsen, O. Hansen, I. Chorkendorff, 2-Photon tandem device for water splitting: comparing photocathode first versus photoanode first designs, Energy Environ. Sci. 7 (2014) 2397–2413. doi:10.1039/C4EE01335B.

[4] F.F. Abdi, L. Han, A.H.M. Smets, M. Zeman, B. Dam, R. van de Krol, Efficient solar water splitting by enhanced charge separation in a bismuth vanadate-silicon tandem photoelectrode, Nat. Commun. 4 (2013) 1–7. doi:10.1038/ncomms3195.

[5] R.H. Coridan, M. Shaner, C. Wiggenhorn, B.S. Brunschwig, N.S. Lewis, Electrical and Photoelectrochemical Properties of WO_3/Si Tandem Photoelectrodes, (2013).

[6] S. Hu, C. Xiang, S. Haussener, A.D. Berger, N.S. Lewis, An analysis of the optimal band gaps of light absorbers in integrated tandem photoelectrochemical water-splitting systems, Energy Environ. Sci. 6 (2013) 2984. doi:10.1039/c3ee40453f.

[7] A.B. Laursen, S. Kegnæs, S. Dahl, I. Chorkendorff, Molybdenum sulfides—efficient and viable materials for electro- and photoelectrocatalytic hydrogen evolution, Energy Environ. Sci. 5 (2012) 5577. doi:10.1039/c2ee02618j.

[8] D. Bae, S. Shayestehaminzadeh, E.B. Thorsteinsson, T. Pedersen, O. Hansen, B. Seger, et al., Protection of Si photocathode using TiO_2 deposited by high power impulse magnetron sputtering for H_2 evolution in alkaline media, Sol. Energy Mater. Sol. Cells. 144 (2016) 758–765. doi:10.1016/j.solmat.2015.10.020.

[9] J.D. Benck, S.C. Lee, K.D. Fong, J. Kibsgaard, R. Sinclair, T.F. Jaramillo, Designing Active and Stable Silicon Photocathodes for Solar Hydrogen Production Using Molybdenum Sulfide Nanomaterials, Adv. Energy Mater. 4 (2014) n/a-n/a.

doi:10.1002/aenm.201400739.
[10] D. Bae, T. Pedersen, B. Seger, M. Malizia, A. Kuznetsov, O. Hansen, et al., Back-illuminated Si photocathode: a combined experimental and theoretical study for photocatalytic hydrogen evolution, Energy Environ. Sci. 8 (2015) 650–660. doi:10.1039/C4EE03723E.
[11] W. Shockley, H.J. Queisser, Detailed balance limit of efficiency of p-n junction solar cells, J. Appl. Phys. 32 (1961) 510–519. doi:10.1063/1.1736034.
[12] M.J. Choi, J.-Y. Jung, M.-J. Park, J.-W. Song, J.-H. Lee, J.H. Bang, Long-term durable silicon photocathode protected by a thin Al_2O_3/SiOx layer for photoelectrochemical hydrogen evolution, J. Mater. Chem. A. 2 (2014) 2928. doi:10.1039/c3ta14443g.
[13] L. Ji, M.D. McDaniel, S. Wang, A.B. Posadas, X. Li, H. Huang, et al., A silicon-based photocathode for water reduction with an epitaxial $SrTiO_3$ protection layer and a nanostructured catalyst., Nat. Nanotechnol. 10 (2014) 84–90. doi:10.1038/nnano.2014.277.
[14] M.G. Kast, L.J. Enman, N.J. Gurnon, A. Nadarajah, S.W. Boettcher, Solution-Deposited F:SnO_2/TiO_2 as a Base-Stable Protective Layer and Antireflective Coating for Microtextured Buried-Junction H2-evolving Si Photocathodes., ACS Appl. Mater. Interfaces. 6 (2014) 22830–7. doi:10.1021/am506999p.
[15] D. V Esposito, I. Levin, T.P. Moffat, a A. Talin, H_2 evolution at Si-based metal-insulator-semiconductor photoelectrodes enhanced by inversion channel charge collection and H spillover., Nat. Mater. 12 (2013) 562–8. doi:10.1038/nmat3626.
[16] S.W. Boettcher, E.L. Warren, M.C. Putnam, E. a. Santori, D. Turner-Evans, M.D. Kelzenberg, et al., Photoelectrochemical hydrogen evolution using Si microwire arrays, J. Am. Chem. Soc. 133 (2011) 1216–1219.
[17] C. Reichel, F. Feldmann, R. M??ller, R.C. Reedy, B.G. Lee, D.L. Young, et al., Tunnel oxide passivated contacts formed by ion implantation for applications in silicon solar cells, J. Appl. Phys. 118 (2015). doi:10.1063/1.4936223.
[18] F. Feldmann, M. Simon, M. Bivour, C. Reichel, M. Hermle, S.W. Glunz, Efficient carrier-selective p- and n-contacts for Si solar cells, Sol. Energy Mater. Sol. Cells. 131 (2014) 100–104. doi:10.1016/j.solmat.2014.05.039.
[19] Y.W. Chen, J.D. Prange, S. Dühnen, Y. Park, M. Gunji, C.E.D. Chidsey, et al., Atomic layer-deposited tunnel oxide stabilizes silicon photoanodes for water oxidation., Nat. Mater. 10 (2011) 539–44. doi:10.1038/nmat3047.
[20] M.J. Kenney, M. Gong, Y. Li, J.Z. Wu, J. Feng, M. Lanza, et al., High-performance silicon photoanodes passivated with ultrathin nickel films for water oxidation., Science. 342 (2013) 836–40. doi:10.1126/science.1241327.
[21] A.G. Scheuermann, J.P. Lawrence, K.W. Kemp, T. Ito, A. Walsh, C.E.D. Chidsey, et al., Design principles for maximizing photovoltage in metal-oxide-protected water-splitting photoanodes, Nat. Mater. (2015) 1–8. doi:10.1038/nmat4451.
[22] P. Stradins, S. Essig, W. Nemeth, B.G. Lee, D. Young, a Norman, et al., Passivated Tunneling Contacts to N-Type Wafer Silicon and Their Implementation into High Performance Solar Cells Preprint, 6th World Conf. Photovolt. Energy Convers. (2014).
[23] W. Kern, The evolution of silicon wafer cleaning technology, J. Electrochem. Soc. 137 (1990) 1887–1892.
[24] B. Seger, S.D. Tilley, T. Pedersen, P.C.K. Vesborg, O. Hansen, M. Graetzel, et al., Silicon protected with atomic layer deposited TiO2: durability studies of photocathodic H2 evolution, RSC Adv. 3 (2013) 25902–25907. doi:10.1039/c3ta12309j.
[25] X. Zhang, A. Thomson, A. Cuevas, Silicon Surface Passivation by Sputtered Aluminium Oxide: Influence of Annealing Temperature and Ambient Gas, ECS Solid State Lett. 3 (2014) N37–N39. doi:10.1149/2.0021412ssl.
[26] J. Schmidt, M. Kerr, Highest-quality surface passivation of low-resistivity p-type silicon

using stoichiometric PECVD silicon nitride, Sol. Energy Mater. Sol. Cells. 65 (2001) 585–591. doi:10.1016/S0927-0248(00)00145-8.
[27] B. Mei, T. Pedersen, P. Malacrida, D. Bae, R. Frydendal, O. Hansen, et al., Crystalline TiO_2 : A Generic and Effective Electron-Conducting Protection Layer for Photoanodes and -cathodes, J. Phys. Chem. C. 119 (2015) 15019–15027. doi:10.1021/acs.jpcc.5b04407.
[28] S. Zhou, X. Pi, Z. Ni, Q. Luan, Y. Jiang, C. Jin, et al., Boron- and phosphorus-hyperdoped silicon nanocrystals, Part. Part. Syst. Charact. 32 (2015) 213–221. doi:10.1002/ppsc.201400103.
[29] Y. Hori, S. Kano, H. Sugimoto, K. Imakita, M. Fujii, Size-Dependence of Acceptor and Donor Levels of Boron and Phosphorus Codoped Colloidal Silicon Nanocrystals, Nano Lett. 16 (2016) 2615–2620. doi:10.1021/acs.nanolett.6b00225.
[30] D. Zhang, A. Tavakoliyaraki, Y. Wu, R.A.C.M.M. Van Swaaij, M. Zeman, Influence of ITO deposition and post annealing on HIT solar cell structures, Energy Procedia. 8 (2011) 207–213. doi:10.1016/j.egypro.2011.06.125.
[31] S. Liang, C. Hsu, C. Tsai, Effect of TCO / c-Si : H Interface Modification on Hydrogenated Microcrystalline Silicon Thin-Film Solar Cells, 2013 (2013).
[32] M.F. Weber, Efficiency of Splitting Water with Semiconducting Photoelectrodes, J. Electrochem. Soc. 131 (1984) 1258. doi:10.1149/1.2115797.
[33] H. Döscher, J.F. Geisz, T.G. Deutsch, J.A. Turner, Sunlight absorption in water – efficiency and design implications for photoelectrochemical devices, Energy Environ. Sci. 7 (2014) 2951–2956. doi:10.1039/c4ee01753f.

Table 1. Structure of samples used in present work and PEC performance under light illumination.

Structure	**Light**[1]	***FG***	V_{OC}**, mV**	J_L[2]**, mA cm^{-2}**	***FF*, %**
Control sample (Control)					
Al/pn$^+$-Si/Ti/TiO_2/Pt	Red	No	489	21.2	60.4
Carrier selective back contact (CS-1)					
Al/nc-Si:B/SiO_X/pn$^+$-Si/Ti/TiO_2/Pt	Red	No	516	22.1	63.6
Carrier selective back & front contacts (CS-2)					
	Red	No	536	22.7	55.3
Al/nc-Si:B/SiO_X/p-Si/SiO_X/nc-Si:P/Ti/TiO_2/Pt	Red	Yes	571	23.6	62.7
	White	Yes	584	33.2	61.3

[1]*White and red light correspond to the simulated light with AM1.5G and AM 1.5G with 635 nm cut-off filters, respectively.*
[2]*Note that J_L corresponds to the photocurrent value measured at 0V vs. RHE*.

Figure 1_revised

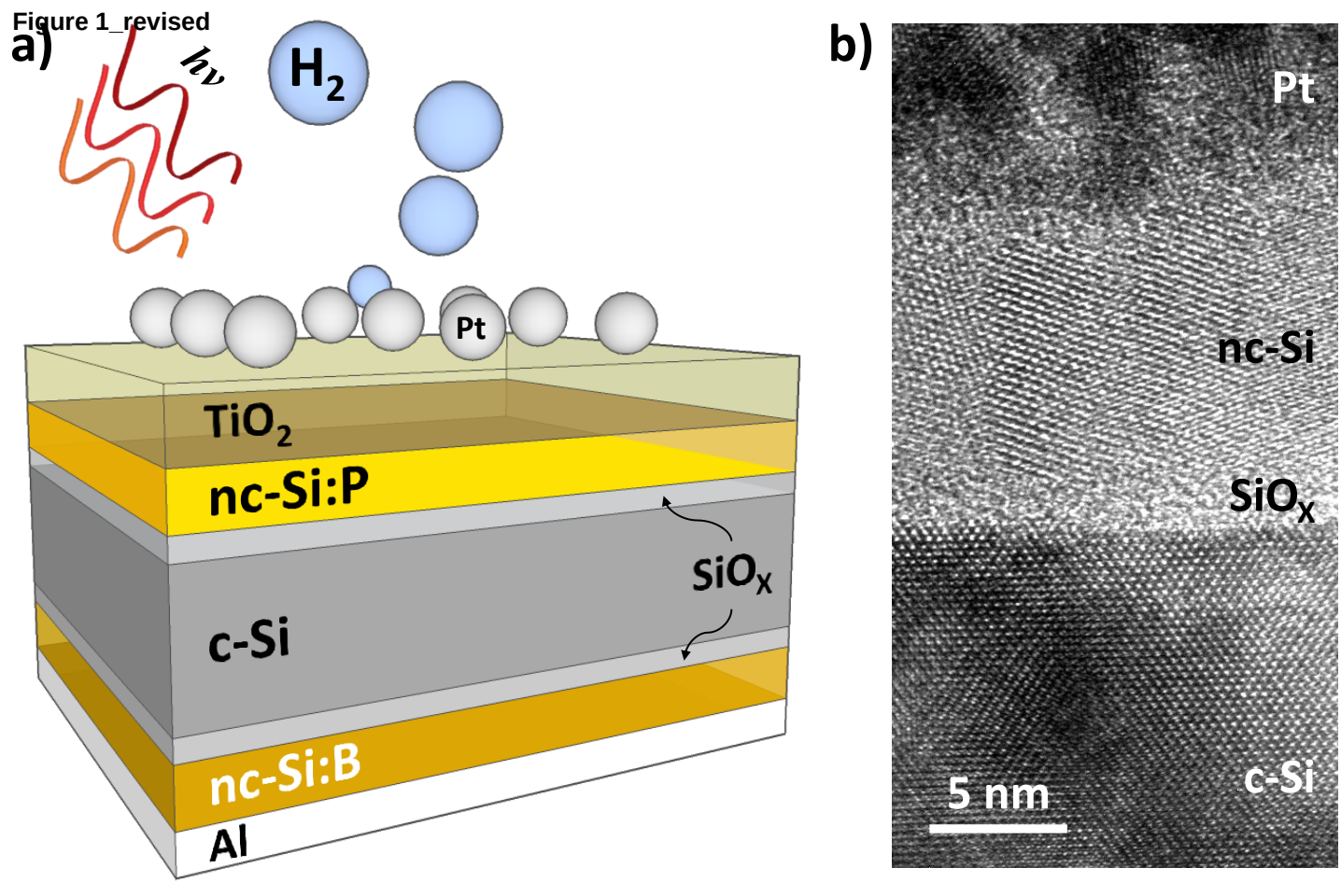

Figure 2_revised

Click here to download high resolution image

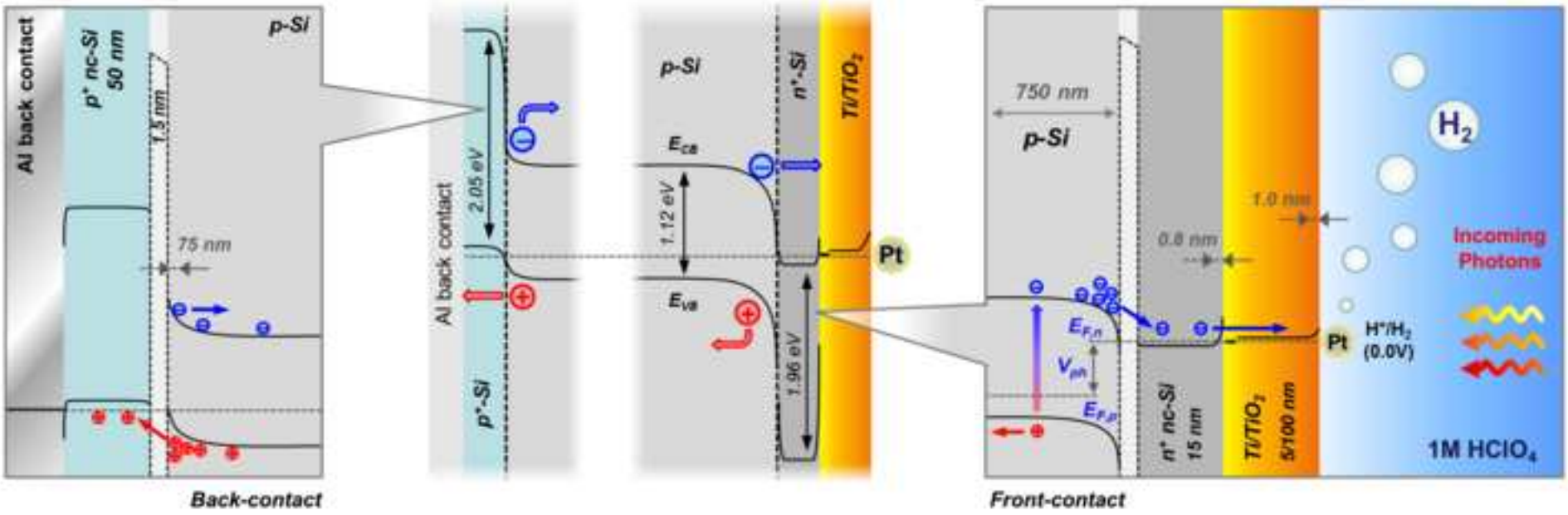

Figure 3 revised

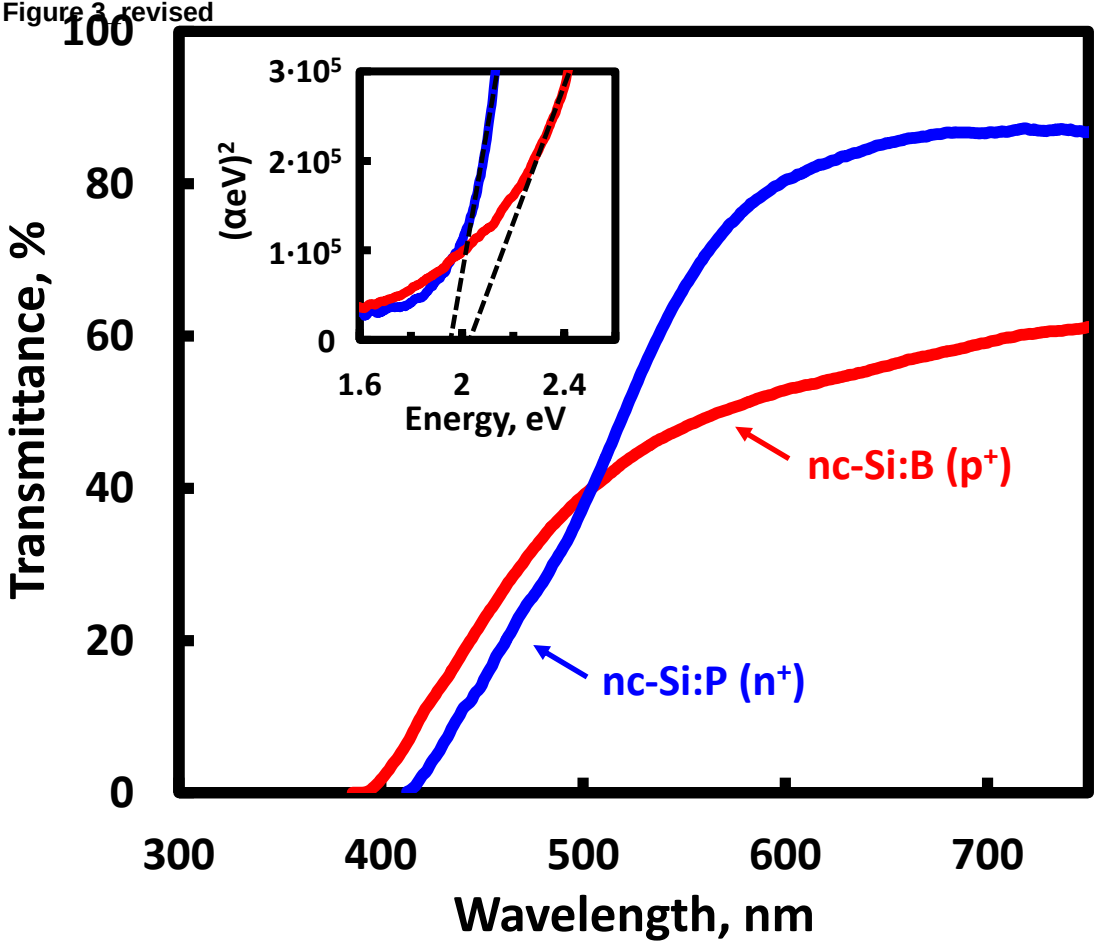

Figure 4

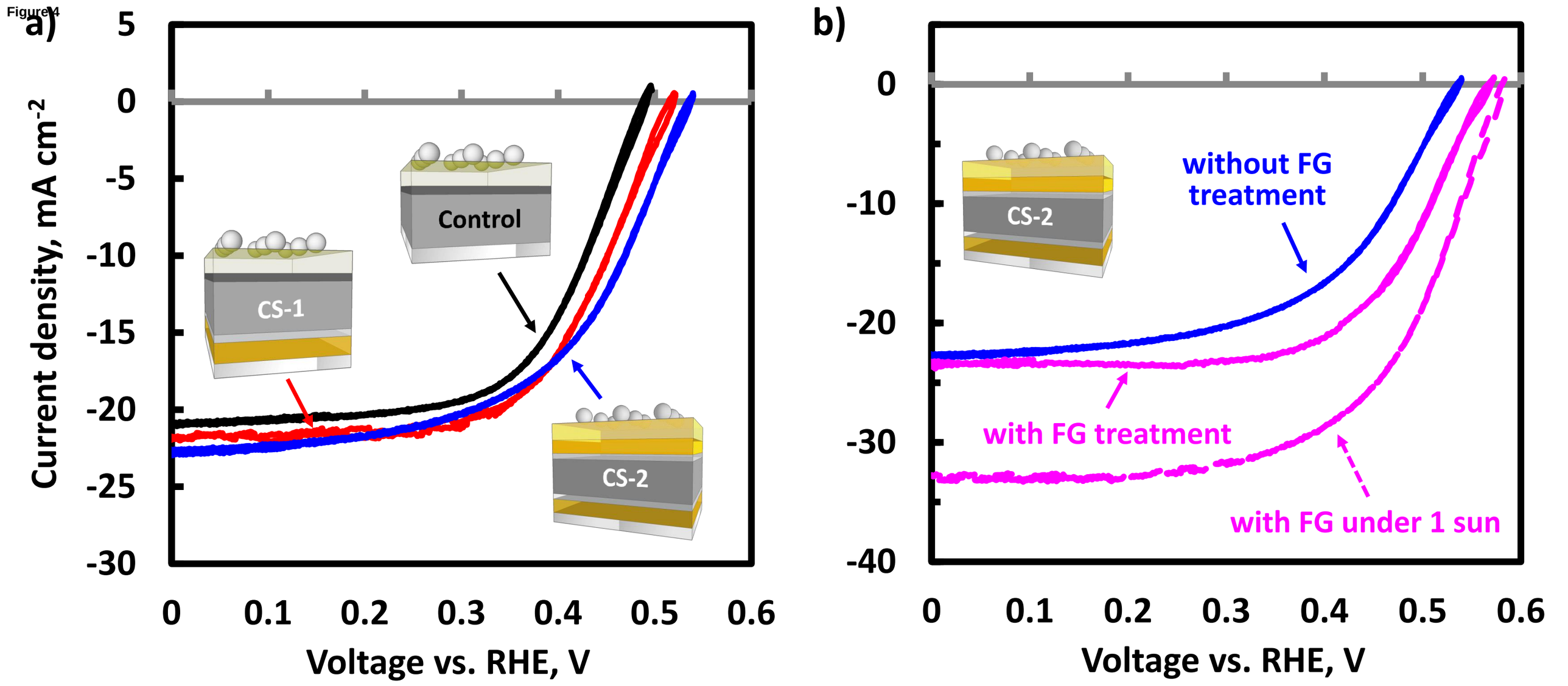
a)
Current density, mA cm-2
5
0
-5
-10
-15
-20
-25
-30
0
0.1
0.2
0.3
0.4
0.5
0.6
Voltage vs. RHE, V
Control
CS-1
CS-2
b)
0
-10
-20
-30
-40
CS-2
without FG treatment
with FG treatment
with FG under 1 sun
0
0.1
0.2
0.3
0.4
0.5
0.6
Voltage vs. RHE, V

Figure 5

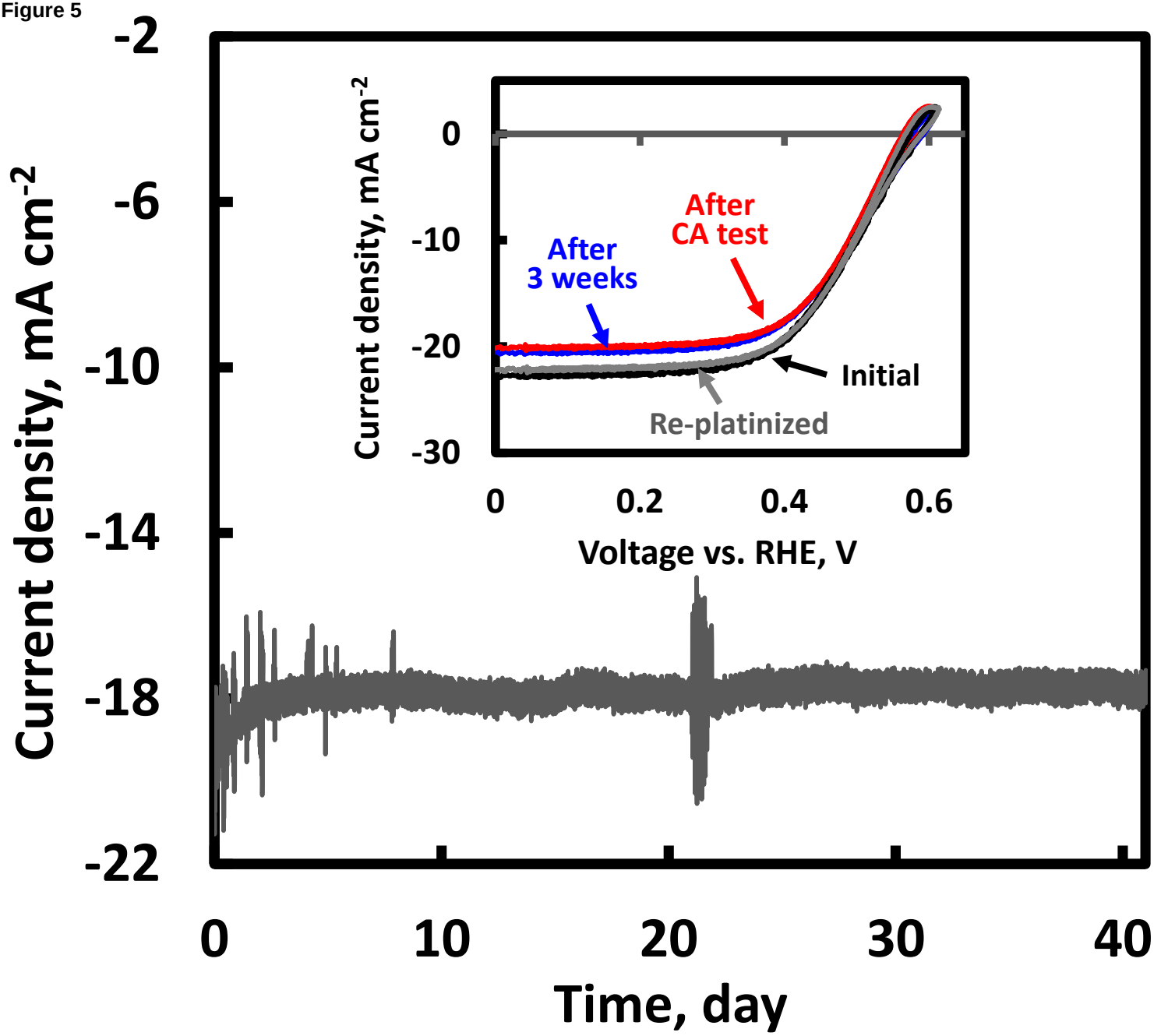
-2
-6
-10
-14
-18
-22
Current density, mA cm-2
0
10
20
30
40
Time, day
0
-10
-20
-30
Current density, mA cm-2
0
0.2
0.4
0.6
Voltage vs. RHE, V
After
3 weeks
After
CA test
Initial
Re-platinized

Supporting Information

Click here to download Supplementary Interactive Plot Data (CSV): Carrier-selective design_supporting information_revised.doc